Metal mesh resonant filters for terahertz frequencies

Arline M. Melo,[1,2,*] Mariano A. Kornberg,[3,6] Pierre Kaufmann,[1,2] Maria H. Piazzetta,[4] Emílio C. Bortolucci,[1] Maria B. Zakia,[1] Otto H. Bauer,[3] Albrecht Poglitsch,[3] and Alexandre M. P. Alves da Silva[5]

[1]Center for Semiconductor Components, Campinas State University, Campinas, Brazil

[2]Center for Radio Astronomy and Astrophysics, CRAAM-Engineering School, Mackenzie Presbyterian University, São Paulo, Brazil

[3]Max-Planck-Institut für extraterrestrische Physik, Garching, Germany

[4]National Synchrotron Light Laboratory, Campinas, Brazil

[5]Department of Microwave and Optics, School of Electrical and Computer Engineering, Campinas State University, Campinas, Brazil

[6]Present address, European Space Research and Technology Centre, Keplerlaan 1, Postbus 299 2200 AG Noordwijk, The Netherlands

*Corresponding author: armame@gmail.com

Received 1 July 2008; revised 18 September 2008; accepted 19 September 2008; posted 19 September 2008 (Doc. ID 97577); published 6 November 2008

The interest in terahertz photometric and imaging measurements has motivated the development of bandpass resonant filters to be coupled to multiple-pixel devices such as bolometer arrays. Resonant grids are relatively simple to fabricate, exhibiting high transmission at the central frequency, a narrow bandpass, and good rejection of the side frequencies of the spectrum. We have fabricated filters centered at different frequencies between 0.4 and 10 THz, using photolithography and electroforming techniques. Transmission measurements have shown center frequencies and bandwidths close to the design predictions. The performance of the filters was found not to be critically dependent on small physical deformations in the mesh, becoming more noticeable at higher frequencies (i.e., for smaller physical sizes). Wider bandwidths, needed to attain higher sensitivities in the continuum, were obtained by changing the design parameters for filters at 2 and 3 THz.

OCIS codes: 220.0220, 120.2440.

1. Introduction

There are increasing demands for experiments in terahertz (THz) frequencies, in different areas such as biotechnology and nanotechnology, space science, security, and plasma diagnostics [1,2]. Those demands have motivated the investigation of radio-frequency filtering methods to select frequency bands in the submillimeter to far-IR spectrum, as for example coupled planar antennas, multilayer IR materials, interferometers and bidimensional structures such as metal mesh filters or frequency-selective surfaces [3].

Metal mesh filters are compact, can exhibit excellent transmission performance, and have the advantage of an easier fabrication process in comparison with other RF tuning possibilities. The bandpass filters exhibit high transmission (higher than 80%) at the central frequency, adjustable bandpass, and good rejection of the sideband frequencies [4–7]. Mesh filters can use different patterns. The most successful use crosses. The filter geometry parameters are G, which represents the periodicity of the cross, K, the width of the cross arms, and L, the cross length. The combinations of these three parameters

0003-6935/08/326064-06$15.00/0

determine the transmission profile. An illustration of a mesh is shown in Fig. 1.

Although it is not much discussed in the literature, the thickness (h) growth control of the metal film might become a critical parameter at higher frequencies in the THz band, where the h parameter may attain values close to the operating wavelengths.

2. Design and Fabrication Process

Metal mesh filters can be fabricated by using different techniques. One micromachining technique uses polymer film as substrate with a metallic thin layer deposited on one side (such as Mylar, metallized polyester). However, plastic films add absorption and have thermal and mechanical limitations for certain applications. Another micromachining procedure employs photolithography followed by electroplating techniques; this procedure produces a metal grown film with an open-space cross format, without absorption, which improves the final filter transmission.

We have used the second technique to fabricate our filters. A first set of filters was fabricated for central frequencies at 0.4, 0.67, 0.85, 2, and 4 THz, for which the designed mesh parameters were derived from Porterfield *et al.* [4], assuming linear variation of the parameters with the frequency in order to obtain a narrower bandpass, about 10% of the central frequencies [8]. A second set of filters was fabricated with larger bandwidth at 2 and 3 THz (around 30% of the central frequency) and at 10 THz (bandpass close to 15% of the central frequency).

The equivalent radiometric system noise temperature in the continuum decreases with the square root of the bandwidth. Therefore larger bandwidths are desirable to obtain better sensitivities. To maximize the resonant mesh bandwidths, we derived their design parameters using a 3D electromagnetic simulator, CST Microwave Studio. We first compared the software response with the actual transmission measurements of the first set of filters to validate the new parameters.

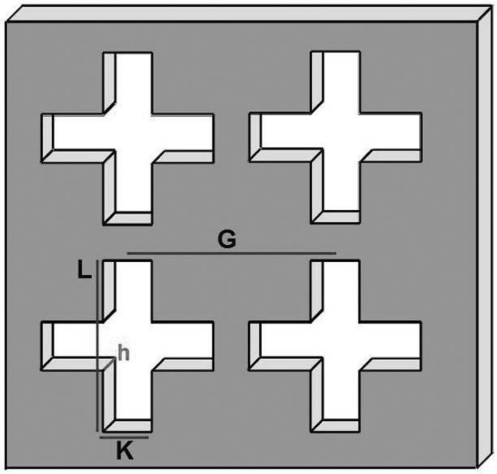

Fig. 1. Illustration of a cross-shaped bandpass filter with geometry parameters G, L, K, and h.

We then searched for the design parameters to produce wider bandpass transmission profiles at 2 and 3 THz. The final parameters were derived by using the simulator software optimizer, which applies the interpolated quasi Newton algorithm. Iterative operations are performed by the optimizer over a range of values for the parameters, using as initial values those from Porterfield *et al.* [4], to obtain the desired central frequency and bandpass.

For the higher frequency (10 THz) the parameters were calculated for optimum performance and are consistent with linear extrapolation with the frequencies from Porterfield *et al.* [4] used before. The measured mesh parameters are shown in Table 1. The frequencies were selected for aerospace applications. The lower frequencies, 0.4, 0.67, and 0.85 THz, correspond to the three last atmospheric windows. The higher frequencies are intended to be used in space experiments, above the atmosphere.

The fabrication processes were performed at the Center for Semiconductor Components (CCS) at Campinas State University, "Renato Archer" Research Center (CenPRA) and National Synchrotron Light Laboratory (LNLS), in Brazil. We used silicon substrates previously prepared with deposited films of silicon oxide, SiO_2 (2 μm thickness), titanium, Ti (200 Å thickness), and gold, Au (1000 Å thickness). In our development we used these substrates prepared with gold film because of its good conductivity for nickel electroplating. The titanium layer was used because of its good adhesion to gold.

In the first set of filters the lithography used SU-8 photoresist, deposited at 1000 rpm for 30 s for 0.4, 0.67, 0.85, and 2 THz, and at 1500 rpm for 30 s for 4 THz, resulting in photoresist thicknesses of 50 and 30 μm, respectively. For the second set of filters the photoresist deposition used 3000 rpm for 30 s, resulting in a photoresist layer of 15 μm. This deposited layer is correlated with the desired metal mesh thickness (Fig. 2).

The samples obtained were submitted to a baking process and then exposed to UV radiation (200 W mercury lamp operating at 220–400 nm) for 30–40 and 7–10 s for the first and second set of filters, respectively. This process sequence prepares the template for the deposition of the metallic material that forms the filter. Figure 2 shows an electron micrograph of two samples with the crosses made of

Table 1. Measured Mesh Parameters for Different Frequencies

Filter	Frequency	L (μm)	K (μm)	G (μm)
F1	405 GHz	370	110	590
F2	670 GHz	225	60	350
F3	850 GHz	175	50	302.5
F4	2 THz	76	22	120
F5[a]	2 THz	81.4	22.6	106.3
F6[a]	3 THz	66.4	12.6	76.5
F7	4 THz	38	10	60
F8	10 THz	3.15	15.4	22.5

[a]Wider bandwidths.

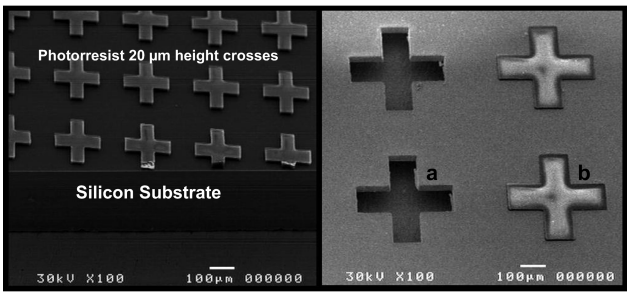

Fig. 2. Left, electron micrograph of the prepared sample for nickel electrodeposition. Right, one example of the final fabricated mesh, a, compared with the crosses made of SU-8 with heights ranging between 10 and 20 μm, b.

SU-8 photoresist, with 10–20 μm height, depending on the filter thickness to be grown. In Figure 2, left-hand side, we can see the silicon substrate and the SU-8 crosses. At the right, a corresponds to the final fabricated mesh result and b the SU-8 crosses above the substrate. We used nickel as the metal material. The electroplating process used a Watts bath of nickel sulfate, nickel chlorine, boric acid, and water, with a current density of 3 A/dcm^2. At this phase the nickel deposition rate could be monitored by using a DekTak3ST profilometer. The last phase is the etching, to remove the photoresist and the layers of SiO_2, titanium, and gold, using a potassium cyanide and HF buffer.

Figure 3 shows the fabrication process steps. Figure 3A shows the prepared sample with SiO_2, titanium, and gold; Fig. 3B shows the sample with photoresist SU-8 deposited; Fig. 3C shows the sample after the UV mask exposition and development (the situation shown in Fig. 2); Fig. 3D shows the metal growth using nickel electroplating; Fig. 3E shows the image of the final nickel film growth waiting for the etching process, which is shown in Fig. 3F, when the filter film is removed from the silicon wafer.

3. Fabrication Results

We first inspected all samples, using a simple microscope, to detect any possible damage. Samples were later analyzed in detail by using an electron microscope to obtain the mesh parameters after the fabrication process. In general, the variations in the parameters were more pronounced for the smaller dimensions, which are more difficult to control during the fabrication process. These variations were associated with the cross pattern resolution in the photolithograph mask, which usually does not correspond exactly to the design specifications. Other variables playing roles are the UV exposition time, the poor mask–substrate contact, and the time for development. Despite of these variables, all filters presented exhibited excellent performance, close to the response expected from the design. In Table 1 we show the measured parameters obtained for the final filters.

Figure 4 shows 2D electron micrographs (top) and at a certain inclination angle (bottom) to show details of the corners, sidewall definition, and the mesh thickness, for three filters samples, 0.67, 2, and 10 THz. From these images we can note that the round features at corners and slight bending of cross arms become more pronounced for frequencies above 2 THz.

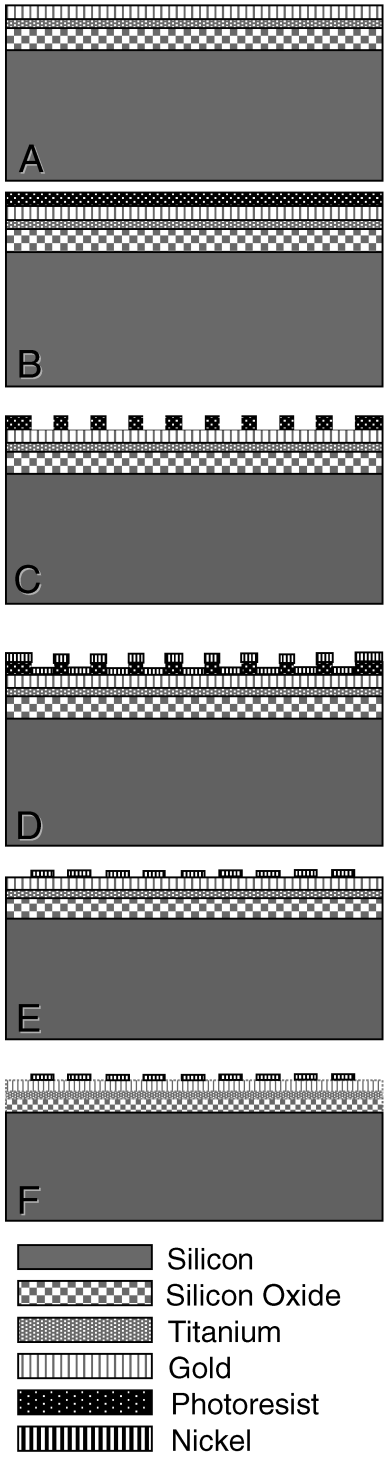

Fig. 3. Steps for the fabrication process: A, prepared substrate with SiO_2, titanium, and fold; B, deposited SU-8 photoresist; C, photolithography process; D, electroplating process; E, development of the photoresist; F, final etching.

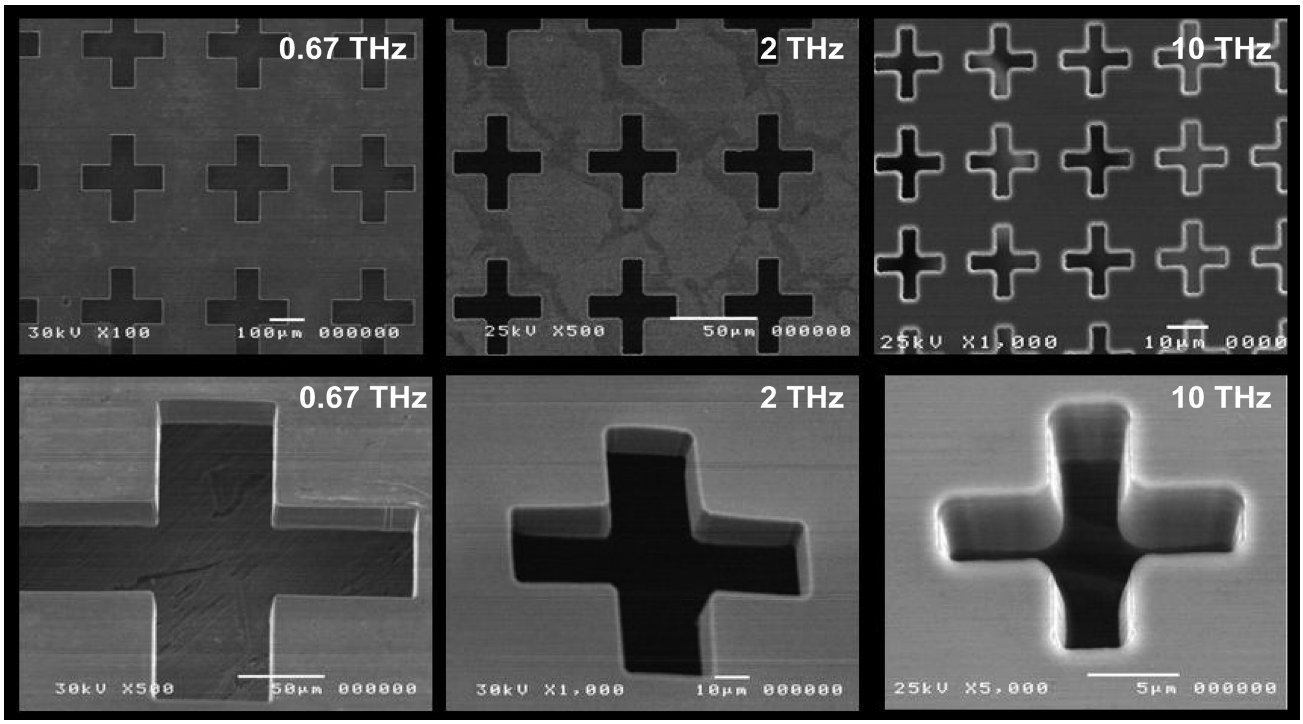

Fig. 4. Electronic micrograph for three filter samples with central frequencies, 0.67, 2, and 10 THz. The enlarged electron micrograph for the same meshes at an angle show more details of the round features at the corners, side wall definition, and slight bending of the cross arms for the 10 THz filter.

4. Transmittance Measurements

The filter transmission was measured at the Max-Planck Institut für extraterrestrische Physik, in Garching, Germany, by using the PACS (Photodetector Array Camera and Spectrometer) development laboratory, part of the Herschel satellite project [9]. The equipment used was a Fourier transform spectrometer employing a mercury lamp as a far- and mid-IR source and a liquid-helium-cooled bolometer as detector. The measured transmission profiles for all filters are shown in Fig. 5. The measured central frequencies, bandwidth, and peak transmittance are listed in Table 2.

The metal layer thickness (h) becomes an important parameter at higher frequencies, where it may become a significant fraction of the wavelength and may add resonance effects, degrading the filter performance. Möller *et al.* [10] indicated the occurrence of resonance effects, denoted "thickness peaks," dependent on the mesh metal film thickness, that become more pronounced at shorter wavelengths, which are not present in our filters' measured profiles.

It has been found that metal mesh thickness can be controlled to a good extent during the electroplating process. The first set of filters fabricated [8] had nickel thickness ranging from 16 to 42 μm. Transmission measurements have shown that their thickness had no important resonant effect up to 4 THz (as shown below). For the second set of filters we had better control of the nickel deposition. The resulting mesh thickness ranged from 7 to 10 μm.

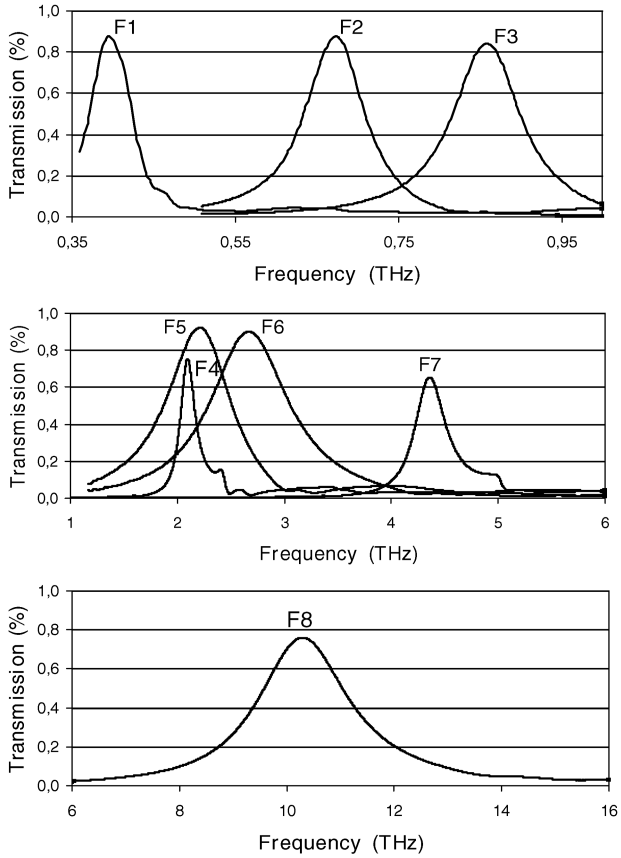

Fig. 5. Transmission frequency response for the fabricated THz filters, exhibiting performances close to the design predictions. The labels correspond to the filters listed in Tables 1 and 2.

Table 2. Measured Mesh Transmission Parameters for Different Mesh Filters

Filter	Frequency	Measured Frequency	Bandwidth (%Fc)	Transmission (%)
F1	405 GHz	395 GHz	17.6	88
F2	670 GHz	674 GHz	14.2	87
F3	850 GHz	858 GHz	14	84
F4[a]	2 THz	2.09 THz	10.7	75
F5[a]	2 THz	2.23 THz	27.8	92.5
F6	3 THz	2.67 THz	28.5	90
F7	4 THz	4.38 THz	8.8	67
F8	10 THz	10.29 THz	13.9	76

[a]Wider bandwidths.

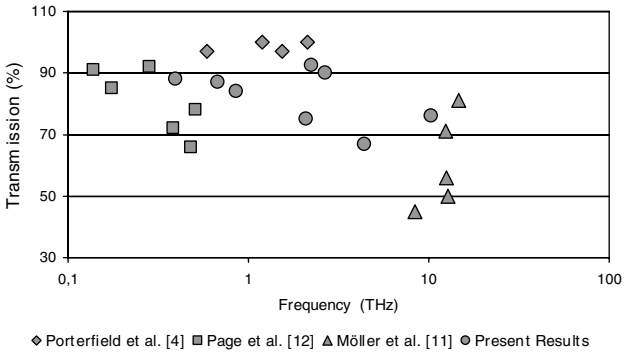

Fig. 6. Mesh filter transmission obtained by different authors, compared with the present results.

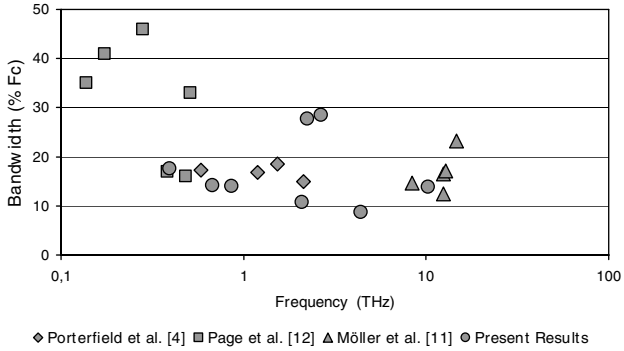

Fig. 7. Comparative half-power bandpass results (in percent of central frequency) obtained by different authors, compared with the present results.

5. Discussion

The filter central frequencies transmission and respective bandwidths were compared with results obtained by other authors [4,11,12], as shown in Figs. 6 and 7, respectively. The 100% peak transmittances reported by Porterfield *et al.* [4] are unlikely because of known intrinsic losses in the interaction of radiation and metallic material.

The mesh design parameters derived from the simulator optimizer applying interpolated quasi Newton algorithm proved to be particularly successful for producing the desired response, presenting wider bandwidths transmission, at 2 and 3 THz. This result is relevant for mesh filtering applications in bolometric photometry requiring higher sensitivity in the continuum. The high transmission obtained for the 10 THz mesh might be attributed to the very thin metal thickness attained (less than 7 μm).

6. Final Remarks

Suspended resonant metallic mesh filters were successfully fabricated for discrete central frequencies ranging from 0.4 to 10 THz. Measured transmission and bandwidths were consistent with the design parameters. It has been shown that the mesh design simulation is a useful tool for obtaining larger bandwidths. The high transmission obtained at 10 THz was possibly related to the small metal thickness attained in fabrication ($\sim$7 μm). The development of THz resonant mesh filters is part of efforts intended to produce and characterize subsystems to be used in solar activity photometry in that range of frequencies, in support of the DESIR (Detection of Eruptive Solar Infrared emission) space experiment on the SMESE (Small Explorer for Solar Eruptions) satellite [13]. Such measurements require sensitivity for detection of small temperature changes against important background emission (small temperature contrasts), which are greatly benefited by the use of large bandwidth suspended metal mesh filters.

We acknowledge the assistance of Rogério Marcon and IFGW, Campinas State University, in obtaining electron micrographs and Angelo Luiz Gobbi, National Synchrotron Light Laboratory, for sample preparation. This research was partially supported by Brazilian agencies Fundação de Amparo à Pesquisa do Estado de São Paulo (FAPESP), Conselho Nacional de Desenvolvimento Científico e Tecnológico (CNPq), Mackpesquisa, and Argentina agency Consejo Nacional de Investigaciones Científicas y Técnicas (CONICET).

References

1. J. F. Federici, B. Schulkin, F. Huang, D. Gary, R. Barat, F. Oliveira, and D. Zimdars, "THz imaging and sensing for security applications—explosives, weapons and drugs," Semicond. Sci. Technol. **20**, S266–S280 (2005).
2. A. Rogalski, "Infrared detectors: status and trends," Prog. Quantum Electron. **27**(2–3), 59–210 (2003).
3. P. F. Goldsmith, "Quasioptical systems," Proc. IEEE 80, 1729–1747 (1992).
4. D. W. Porterfield, J. L. Hesler, R. Densing, E. R. Mueller, T. W. Crowe, and R. M. Weikle II, "Resonant metal mesh bandpass filters for the far infrared," Appl. Opt. **33**, 6046–6052 (1994).
5. V. P. Tomaselli, D. C. Edewaard, P. Gillan, and K. D. Möller, "Far infrared bandpass filters from cross shaped grids," Appl. Opt. **20**, 1361–1366 (1981).
6. R. Ulrich, "Far infrared properties of metallic mesh and its complementary structure," Infrared Phys. **7**, 37–50 (1967).
7. S. T. Chase and R. D. Joseph, "Resonant array bandpass filters for the far infrared," Appl. Opt. **22**, 1775–1779 (1983).
8. A. M. Melo, O. H. Bauer, E. C. Bortolucci, P. Kaufmann, M. Kornberg, M. H. Piazzetta, A. Poglitsch, A. M. P. A. da Silva, and M. B. Zakia, "The development of RF band-pass resonant mesh filters for the THz range," in *International*

Workshop on Telecommunications Proceedings (Inatel, 2007), pp. 256–258.
9. A. Poglitsch, C. Waelkens, O. H. Bauer, J. Cepa, H. Feuchtgruber, T. Henning, C. van Hoof, F. Kerschbaum, D. Lemke, E. Renotte, L. Rodriguez, P. Saraceno, and B. Vandenbussche, "The photodetector array camera and spectrometer (PACS) for the Herschel Space Observatory," Proc. SPIE **6265**, 62650B (2006).
10. K. D. Möller, O. Sternberg, H. Grebel, and P. Lalanne, "Thick inductive cross shaped metal mesh," J. Appl. Phys. **91**, 9461–9465 (2002).
11. K. D. Möller, J. B. Warren, J. B. Heaney, and C. Kotecki, "Cross-shaped bandpass filters for the near- and mid-infrared wavelength regions," Appl. Opt. **35**, 6210–6215 (1996).
12. L. A. Page, E. S. Cheng, B. Golubovic, J. Gundersen, and S. S. Meyer, "Millimeter–submillimeter wavelength filter system," Appl. Opt. **33**, 11–23 (1994).
13. J.-C. Vial, F. Auchère, J. Chang, C. Fang, W. Q. Gan, K.-L. Klein, J.-Y. Prado, F. Rouesnel, A. Sémery, G. Trottet, and C. Wang, "SMESE (Small Explorer for Solar Eruptions): a microsatellite mission with combined solar payload," Adv. Space Res. **41**, 183–189 (2008).